Comput Geosci (2015) 19:569–583
DOI 10.1007/s10596-015-9480-0

ORIGINAL PAPER

A reactive transport benchmark on modeling biogenic uraninite re-oxidation by Fe(III)-(hydr)oxides

S. Sevinç Şengör[1] · K. Ulrich Mayer[2] · Janek Greskowiak[3] · Christoph Wanner[4] · Danyang Su[2] · Henning Prommer[5,6,7]

Published online: 13 May 2015

Abstract A reactive transport benchmark on uranium (U) bioreduction and concomitant reoxidation has been developed based on the multicomponent biogeochemical reaction network presented by Spycher et al. (*Geochim Cosmochim Acta* 75:4426–4440, 2011). The benchmark problem consists of a model inter-comparison starting with the numerical simulations of the original batch experiments of Sani et al. (*Geochim Cosmochim Acta* 68:2639–2648, 2004). The batch model is then extended to 1D and 2D reactive transport models, designed to evaluate the model results for the key biogeochemical reaction processes and their coupling with physical transport. Simulations are performed with four different reactive transport simulators: PHREEQC, PHT3D, MIN3P, and TOUGHREACT. All of the simulators are able to capture the complex biogeochemical reaction kinetics and the coupling between transport and kinetic reaction network successfully in the same manner. For the dispersion-free variant of the problem, a 1D-reference solution was obtained by PHREEQC, which is not affected by numerical dispersion. PHT3D using the sequential non-iterative approach (SNIA) with an explicit TVD scheme and MIN3P using the global implicit method (GIM) with an implicit van Leer flux limiter provided the closest approximation to the PHREEQC results. Since the spatial weighting schemes for the advection term and numerical dispersion played an important role for the accuracy of the results, the simulators were further compared using different solution schemes. When all codes used the same spatial weighting scheme with finite-difference approximation, the simulation results agreed very well among all four codes. The model intercomparison for the 2D-case demonstrated a high level of sensitivity to the mixing of different waters at the dispersive front. Therefore this benchmark problem is well-suited to assess code performance for mixing-controlled reactive transport models in conjunction with complex reaction kinetics.

Keywords Reactive transport benchmark · Uranium · Bioremediation · Reoxidation · Numerical dispersion

✉ S. Sevinç Şengör
sssengor@gmail.com

[1] Civil and Environmental Engineering Department, Southern Methodist University, Dallas, TX 75275, USA

[2] Department of Earth, Ocean and Atmospheric Sciences, The University of British Columbia, Vancouver, BC, Canada

[3] Department of Biology and Environmental Sciences, University of Oldenburg, Oldenburg, Germany

[4] Earth Sciences Division, Lawrence Berkeley National Laboratory, 1 Cyclotron Road, Berkeley, CA 94720, USA

[5] CSIRO Land and Water, Private Bag No. 5, Wembley, WA 6913, Australia

[6] School of Earth and Environment, University of Western Australia, Crawley, WA, Australia

[7] National Centre for Groundwater Research and Training (NCGRT), Flinders University, AdelaideGPO Box 2100SA 5001, Australia

1 Introduction

Uranium (U) is considered as a primary constituent at various U.S. Department of Energy (DOE) waste sites and many ecosystems worldwide as it can pose a significant hazard to human health and natural environments.

Understanding the processes that control the stability and mobility of uranium in groundwater systems is crucial for minimizing the risk of it's reaching critical receptors [1]. In general, oxidized U(VI) is significantly more soluble than U(IV). Therefore the reduction of U(VI) to U(IV) is considered to be an attractive option to stabilize U at affected sites [2, 3]. Under suitable geochemical conditions specific microbial groups such as sulfate reducing bacteria (SRB) can reduce soluble U(VI) to insoluble U(IV), leading to the precipitation of uraninite (UO_2) [4–6]. Therefore, a promising remediation strategy is to immobilize U by injecting soluble electron donors such as lactate, which promotes and allows maintaining the bacterial activity that causes a shift towards more reducing geochemical conditions under which uraninite is stable. However, Sani et al. [7] have shown that once electron donors are entirely consumed, uraninite may be reoxidized in the presence of Fe(III)-(hydr)oxides, therefore potentially limiting the sustainability of cleanup efforts for U(VI)-contaminated groundwater. To assess U(VI) bioreduction with concomitant UO_2 reoxidation in the presence of hematite or ferrihydrite within a quantitative framework, a suitable conceptual model and a corresponding reaction network was developed by Spycher et al. [8], based on experiments earlier reported by Sani et al. [7]. This reaction network considers sulfate reduction in conjunction with lactate oxidation as well as the abiotic and microbially mediated reductive dissolution of Fe(III) solids by sulfide.

The benchmark problem presented in this paper directly adopts the reaction network that was developed and described in full detail by Spycher et al. [8] and explores the hydrogeochemical patterns that develop under steady-state and transient groundwater flow conditions. A simplified conceptual model illustrating the major biotic and abiotic reactions considered in the benchmark problem is given in Fig. 1. The main challenge of this benchmark is the complexity of the biogeochemical reaction network, which includes various parallel, sequential and competing kinetic reactions with a strong interdependency of these processes. In addition, some of these reactions are mixing controlled and the reaction progress as well as the resulting solution chemistry are highly sensitive to physical mixing and therefore potentially compromised by numerical dispersion. This causes a strong coupling between the physical transport and geochemical reaction processes. Inaccurate solutions of the physical transport processes will be more pronounced in multi-dimensional problems, where finer grid resolutions that typically minimize numerical dispersion come at larger computational costs and pragmatic choices have to be made to attain sufficient accuracy

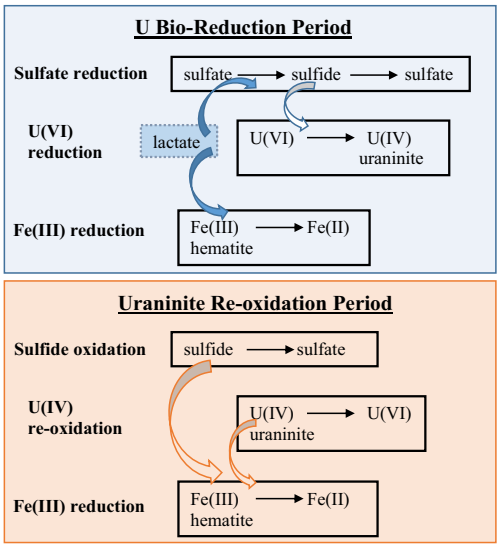

Fig. 1 Simplified conceptual model illustrating the biotic and abiotic reaction network considered in the benchmark for the batch system, 1D and 2D reactive transport simulations. Note that these reactions are coupled to the precipitation/dissolution of solid phases: biogenic uraninite ($UO_{2(bio)}$), hematite (Fe_2O_3), siderite ($FeCO_3$), and disordered mackinawite (FeS_m) as well as sulfur ($S_{(s)}$) as described in the text

at reasonable computational costs. The benchmark problem consists of three parts:

1. Numerical simulation of the batch experiments by Sani et al. [7], based on the biogeochemical reaction network developed by Spycher et al. [8].
2. Extension of part (1) to a 1D reactive transport simulation, characterized by a steady-state flow and a generally constant inflow of an U(VI)-containing solution, except for a temporary amendment of lactate.
3. The extension of part (2) to a 2D reactive transport simulation model with a temporary injection of lactate in the center of the model domain.

Although various models have previously been used to investigate U bioreduction and also coupled oxidation processes, a systematic model intercomparison capturing similarly complex coupled processes has not been conducted to date. Therefore, the aim of this paper is to provide and describe a benchmark problem which allows testing and comparing reactive transport simulations that involve a set of complex biogeochemical reactions under conditions where physical transport, mixing and its accurate simulation plays an important role for the evolution of the biogeochemical patterns. Our comparison illustrates how the four different reactive transport simulators PHREEQC [9], PHT3D [10], MIN3P [11], and TOUGHREACT [12, 13] and their varying model formulations allow to address the challenges of the benchmark problem.

2 Problem definition and parameters

2.1 Reaction network description

The proposed benchmark adopts the reaction network defined by Spycher et al. [8]. Their model was developed to derive a quantitative description of earlier experiments by Sani et al. [7]. The reaction network, as illustrated in Fig. 1, consists of a mixture of equilibrium and kinetically controlled homogeneous and heterogeneous reactions.

2.1.1 Kinetically controlled reactions

Several of the key reactions were assumed to be kinetically controlled and the corresponding rate formulations, as discussed below, were accordingly incorporated into the reaction databases of the various simulators. Kinetically controlled reactions include sulfate bioreduction, Fe(III) bioreduction, U(VI) bioreduction, Fe(III) reduction by HS, U(IV) oxidation by Fe(III), and precipitation/dissolution of sulfur. The stoichiometric relationships of those kinetic reactions are:

Lactate degradation coupled to sulfate reduction (biotic)

$$2\,C_3H_5O_3^- + SO_4^{-2} \rightarrow 2\,CH_3COO^- + 2CO_3^{-2} + HS^- + 3\,H^+ \qquad \log(K_{25C}) = 2.252 \tag{1}$$

Lactate degradation coupled to Fe(III) reduction (biotic)

$$C_3H_5O_3^- + 4Fe^{+3} + 2\,H_2O \rightarrow CH_3COO^- + CO_3^{-2} + 4Fe^{+2} + 6\,H^+ \qquad \log(K_{25C}) = 72.652 \tag{2}$$

Lactate degradation coupled to sulfate (Eq. 1) and/or Fe(III) reduction (Eq. 2) is assumed to be microbially mediated and the rate R_{Lac} of each of the processes is modeled using a conventional dual-Monod rate law with biomass growth [8, 14]:

$$R_{\mathrm{Lac}} = v_{\max} C_{\mathrm{BM}} \frac{C_{\mathrm{ED}}}{k_{\mathrm{ED}} + C_{\mathrm{ED}}} \frac{C_{\mathrm{EA}}}{k_{\mathrm{EA}} + C_{\mathrm{EA}}} f_{\mathrm{G}} \tag{3}$$

With

$$R_{\mathrm{BM}} = Y_{\mathrm{BM}} R - k_{\mathrm{dec}} C_{\mathrm{BM}} \tag{4}$$

$$f_G = (1 - Q/K) \tag{5}$$

where C is concentration and the subscripts EA, ED, and BM represent electron acceptor (either Fe(III) or sulfate), electron donor, and biomass, respectively, k is a half saturation constant in units of C, $v_{\max}$ is the rate of maximum substrate utilization (in units of moles per time, per biomass), Y_{BM} is the microbial yield coefficient (in units of biomass per substrate), k_{dec} is the cell decay rate (in units of per time), and f_{G} is the affinity term which varies between 1 (far from equilibrium) to 0 (equilibrium). Q is the ion activity product and K is the equilibrium constant of each reaction. Note that although the lactate degradation reaction stoichiometries (Eqs. 1 and 2) do not explicitly include biomass generation, microbial concentrations are still simulated.

U(VI) reduction (combined abiotic and biotic)

$$4\,UO_2^{+2} + HS^- + 7\,H^+ \rightarrow 4\,U^{+4} + SO_4^{-2} + 4\,H_2O \qquad \log(K_{25C}) = 2.51 \tag{6}$$

The corresponding rate R_{Ured} of the reaction is computed from

$$R_{\mathrm{Ured}} = k_{\mathrm{Ured}} \frac{C_{\mathrm{ED}}}{k_{\mathrm{ED}} + C_{\mathrm{ED}}} f_{\mathrm{G}} \tag{7}$$

where k_{Ured} and k_{ED} were adjusted to reproduce the observed experimental results. Spycher et al. [8] proposed to use this rate expression instead of the Monod-type expression employed in Eq. (3). By doing so they minimized the number of adjustable model parameters while implicitly assuming that the reaction progress may be limited by lactate (C_{ED}) availability, but not by electron acceptor availability. Other abiotic reactions include:

U(IV) oxidation by Fe(III)(abiotic):

$$U^{+4} + 2\,Fe^{+3} + 2\,H_2O \rightarrow UO_2^{+2} + 2\,Fe^{+2} + 4\,H^+ \qquad \log(K_{25C}) = 16.972 \tag{8}$$

HS^- oxidation by Fe(III) (abiotic):

$$8\,Fe^{+3} + HS^- + 4\,H_2O \rightarrow 8\,Fe^{+2} + SO_4^{-2} + 9\,H^+ \qquad \log(K_{25C}) = 70.397 \tag{9}$$

Precipitation/dissolution of sulfur:

$$2Fe^{+3} + HS^- \rightarrow 2Fe^{+2} + S_{(s)} + H^+ \qquad \log(K_{25C}) = 28.12 \tag{10}$$

The rates of the reactions defined by Eqn. (8)–(10) are determined from

$$R = r f_G, \tag{11}$$

where r (in units of molar per time) is assumed to be constant. These reactions are operating close to equilibrium and the direction of the reaction (dissolution or precipitation) might

be reversed over time, depending on whether the ion activity product, Q, is smaller or greater than K. In order to ensure that f_G remains between 0 (equilibrium) and 1 (far from equilibrium), this term was set as $f_G=-(1-K/Q)$ in the case of reversal. The precipitation/dissolution of elemental sulfur ($S_{(s)}$) was also treated as a kinetically controlled reaction (Eq. 10), to yield results consistent with experiments [8].

Note that the simulated reaction network remained the same for all three parts of the benchmark problem, i.e., the batch model as well as the 1D and 2D reactive transport models. However, the reaction rate constants for the above described kinetic reactions were modified in the 1D and 2D transport simulations in order to account for the typically lower reaction rates that are observed in flow-through systems compared to well-mixed batch systems (e.g., Park et al. [15]). Thermodynamic data for the aqueous speciation reactions are given in Table 1 and the kinetic parameters for each of the kinetic reactions are given in Table 2.

2.1.2 Equilibrium reactions

Generally all homogenous, i.e., aqueous complexation reactions were assumed to proceed fast and were therefore modeled as equilibrium reactions. Following Spycher et al. [8], a subset of the precipitation/dissolution reactions were also implemented as equilibrium reactions, where the precipitation/dissolution reactions of solid phases were assumed to be limited only by the rate of the aqueous reactions described above [8]. The minerals for which equilibrium was assumed included biogenic uraninite ($UO_{2(bio)}$), hematite (Fe_2O_3), siderite ($FeCO_3$), and disordered mackinawite (FeS_m). Equilibrium mineral dissolution and precipitation reactions are described using the mass action equation:

$$K_m = \prod_{j=1}^{Nc} \left(\gamma_j C_j\right)^{\nu_{mj}} \tag{12}$$

where K_m is the equilibrium constant for the mineral dissolution reaction (assuming unit activity of solid phases), N_c is the number of primary species considered, subscript m refers to minerals, and ν_{mj} are the stoichiometric coefficients of primary species j in mineral m. Note that alternatively, these reactions may be described as kinetically controlled reactions. This approach is, for example, employed in MIN3P, whereby large rate constants are used to obtain fast reactions to obtain quasi-equilibrium conditions.

Activity coefficients of aqueous species are calculated using the Davies equation for PHREEQC and PHT3D, and the extended Debye-Hückel equation for MIN3P and TOUGHREACT simulators. As the benchmark problem presented here is mainly dominated by complex biogeochemical reaction kinetics and transport processes (as well as the

Table 1 Thermodynamic data for aqueous speciation reactions

Aqueous speciation reaction	Log K
$H^+ + Acetate^- = H(Acetate)$	4.757
$H^+ + CO_3^{-2} = HCO_3^-$	10.329
$2H^+ + CO_3^{-2} = CO_2 + H_2O$	16.681
$Ca^{+2} + HCO_3^- = CaCO_3 + H^+$	−7.002
$Ca^{+2} + Cl^- = CaCl^+$	−.696
$Ca^{+2} + 2Cl^- = CaCl_2$	−0.644
$Ca^{+2} + HCO_3^- = CaHCO_3^+$	1.047
$Ca^{+2} + H_2O = CaOH^+ + H^+$	−12.85
$Ca^{+2} + Sulfate^{-2} = Ca\ Sulfate$	2.111
$Fe^{+2} + 2CO_3^{-2} = Fe(CO_3)_2^{-2}$	7.45
$Fe^{+2} + 3H_2O = Fe(OH)_3^- + 3H^+$	−32.962
$Fe^{+2} + 4H_2O = Fe(OH)_4^{-2} + 4H^+$	−46
$Fe^{+3} + 2\ Sulfate^{-2} = Fe(Sulfate)_2^-$	3.214
$2Fe^{+3} + 2H_2O = Fe_2(OH)_2^{+4} + 2H^+$	−7.283
$3\ Fe^{+3} + 4\ H_2O = Fe_3(OH)_4^{+5} + 4\ H^+$	−6.3
$Fe^{+2} + CO_3^{-2} = FeCO_3$	5.45
$Fe^{+2} + Cl^- = FeCl^+$	−0.16
$Fe^{+3} + Cl^- = FeCl^{+2}$	1.48
$Fe^{+2} + 2Cl^- = FeCl_2$	−2.45
$Fe^{+2} + CO_3^{-2} + H^+ = FeHCO_3^+$	11.799
$Fe^{+2} + H_2O = FeO + 2H^+$	−20.405
$Fe^{+3} + H_2O = FeO^+ + 2H^+$	−5.65
$Fe^{+3} + 2H_2O = FeO2^- + 4H^+$	−21.62
$Fe^{+2} + H_2O = FeOH^+ + H^+$	−9.315
$Fe^{+3} + H_2O = FeOH^{+2} + H^+$	−4.38
$Fe^{+2} + HS^- = FeS + H+$	−2.2
$Fe^{+2} + Sulfate^{-2} = Fe\ Sulfate$	2.2
$Fe^{+3} + Sulfate^{-2} = Fe\ Sulfate^+$	1.93
$H^+ + HS^- = H_2S$	7.02
$2H^+ + Sulfate^{-2} = H_2\ Sulfate$	0
$Fe^{+3} + 2H_2O = HFeO_2 + 3H^+$	−12.018
$Fe^{+2} + 2H_2O = HFeO_2^- + 3H^+$	−33.988
$H^+ + Sulfate^{-2} = H\ Sulfate-$	1.99
$4Mg^{+2} + 4H_2O = Mg_4(OH)_4^{+4} + 4H^+$	−39.75
$Mg^{+2} + CO_3^{-2} = MgCO_3$	2.98
$Mg^{+2} + Cl^- = MgCl^+$	−0.1349
$Mg^{+2} + H^+ + CO_3^{-2} = MgHCO_3^+$	11.339
$Mg^{+2} + H_2O = MgOH^+ + H^+$	−11.397
$Mg^{+2} + Sulfate^{-2} = Mg\ Sulfate$	2.26
$Na^+ + CO_3^{-2} = NaCO_3^-$	1.27
$Na^+ + Cl^- = NaCl$	−0.777
$Na^+ + H^+ + CO_3^{-2} = NaHCO_3$	10.079
$Na^+ + H_2O = NaOH + H^+$	−14.18
$Na^+ + Sulfate^{-2} = Na\ Sulfate^-$	0.73
$HS^- = S^{-2} + H^+$	−12.918
$11Uranyl^{+2} + 6CO_3^{-2} + 12H_2O = (Uranyl)_{11}(CO_3)_6(OH)_{12}^{-2} + 12H^+$	36.12
$2Uranyl^{+2} + 2H_2O = (Uranyl)_2(OH)_2^{+2} + 2H^+$	−5.659
$2Uranyl^{+2} + CO_3^{-2} + 3H_2O = (Uranyl)_2(CO_3)(OH)^{3-} + 3H^+$	−0.916

Table 1 (continued)

Aqueous speciation reaction	Log K
$2Uranyl^{+2}+H_2O=(Uranyl)_2OH^{+3}+H^+$	−2.729
$3Uranyl^{+2}+6CO_3^{-2}=(Uranyl)_3(CO3)_6^{-6}$	53.88
$3Uranyl^{+2}+4H_2O=(Uranyl)_3(OH)_4^{+2}+4H^+$	−11.96
$3Uranyl^{+2}+5H_2O=(Uranyl)_3(OH)_5^{+}+5H^+$	−15.62
$3Uranyl^{+2}+7H_2O=(Uranyl)_3(OH)_7^{-}+7H^+$	−32.2
$3Uranyl^{+2}+CO_3^{-2}+3H_2O=(Uranyl)_3O(OH)_2(HCO_3)^{+}+3H^+$	0.583
$4Uranyl^{+2}+7H_2O=(Uranyl)4(OH)_7^{+}+7H^+$	−21.995
$U^{+4}+4CO_3^{-2}=U(CO_3)_4^{-4}$	35.05
$U^{+4}+5CO_3-2=U(CO_3)_5^{-6}$	33.82
$U^{+4}+2Sulfate^{-2}=U(Sulfate)_2$	10.5
$Uranyl^{+2}+2Sulfate^{-2}=Uranyl(Sulfate)_2^{-2}$	4.3
$U^{+4}+Cl^{-}=UCl^{+3}$	1.697
$Uranyl^{+2}+Cl^{-}=Uranyl\ Cl^{+}$	0.141
$Uranyl^{+2}+2Cl^{-}=Uranyl\ Cl_2$	−1.146
$Uranyl^{+2}+Sulfate^{-2}=Uranyl\ Sulfate$	3.18
$Uranyl^{+2}+H_2O=Uranyl\ OH++H^+$	−5.217
$2H_2O+Uranyl^{+2}=Uranyl(OH)_2+2H^+$	−12.152
$Uranyl^{+2}+3H_2O=Uranyl\ (OH)_3^{-}+3H^+$	−20.246
$Uranyl^{+2}+4H_2O=Uranyl(OH)_4^{-2}+4H^+$	−32.4
$U^{+4}+H_2O=UOH^{+3}+H^+$	−0.541
$U^{+4}+2H_2O=U(OH)_2^{+2}+2H^+$	−1.091
$U^{+4}+3H_2O=U(OH)_3++3H^+$	−4.69
$U^{+4}+4H_2O=U(OH)_4+4H^+$	−9.98
$U^{+4}+Sulfate^{-2}=USulfate^{+2}$	6.6
$Uranyl^{+2}+CO_3^{-2}=Uranyl\ CO_3$	9.94
$Uranyl^{+2}+2CO_3^{-2}=Uranyl(CO_3)_2^{-2}$	16.61
$Uranyl^{+2}+3CO_3^{-2}=Uranyl(CO_3)_3^{-4}$	21.84
$Ca^{+2}+Uranyl^{+2}+3CO_3^{-2}=Ca\ Uranyl(CO_3)_3^{-2}$	27.18
$2Ca^{+2}+Uranyl^{+2}+3CO_3^{-2}=Ca_2\ Uranyl(CO_3)_3$	30.7

numerical schemes for the transport solution), variations in computed activity coefficients with the different codes have negligible effect on the results. The activity coefficient parameters for the codes are provided in the databases supplied in the Supporting Material.

2.2 Transport processes

In parts 2 and 3 of the proposed benchmark, numerical simulation of the batch experiments using the multicomponent biogeochemical reaction network described above is extended to include flow and transport of solutes. The governing equation describing the advective-dispersive reactive transport of *i*th (mobile) aqueous component is:

$$\frac{\partial(\theta C_i)}{\partial t} = \nabla\cdot(\theta D\nabla C_i) - \nabla\cdot(\theta v C_i) - q_s C_i^s + \theta r_{react,i} \tag{13}$$

where $\nabla = \left(\frac{\partial}{\partial x}, \frac{\partial}{\partial y}, \frac{\partial}{\partial z}\right)$ and D is the hydrodynamic dispersion coefficient tensor and v is the pore velocity vector $v=(v_x, v_y, v_z)$ with v_x, v_y, and v_z are the pore velocities in x, y, and z direction.

The concentration change for immobile entities, e.g., bacteria and/or minerals is computed by:

$$\frac{\partial C_i}{\partial t} = r_{\mathrm{react},i} \tag{14}$$

where q_s is a volumetric flow rate per unit volume of aquifer representing fluid sources (positive) and sinks (negative), θ is the porosity of the subsurface medium, C_i^s is the concentration of the source or sink flux, $r_{\mathrm{react},i}$ is a source/sink rate due to chemical reaction and C_i is the total aqueous component concentration of the *i*th component [16, 17]. A more detailed description of the codes and their capabilities is provided in Steefel et al. [18].

2.3 Flow and transport model setup

2.3.1 1D model

The 1D benchmark problem was defined as an 18-m-long column with a nominal grid resolution of 0.125 m (see Fig. 2). However, the grid size of the first cell at the left hand boundary was reduced (0.0625 m) for all simulators (except PHREEQC) to match the exact locations of the observation

Table 2 Calibrated kinetic parameters used for the simulation of U(VI) bioreduction in the presence of hematite (from Spycher et al. 2011 [8])

Process	Reaction	Rate Law	q (mol/s/mg_{cells}) or r (mol/s)	k_{ED} (mol/L)	k_{EA} (mol/L)	Y_{BM} (mg_{cells}/mol)	k_{DEC} (1/s)
Sulfate bioreduction	(1)	(3)	1e-8/100	2×10^{-2}	2×10^{-2}	1,600	1e-8/100
Fe(III) bioreduction	(2)	(3)	1e-11/100	2×10^{-2}	10^{-20} [a]	1,600	1e-8/100
U(VI) bioreduction	(6)	(7)	8e-11/100	4×10^{-2}			
Fe(III) reduction by HS	(9)	(11)	0.45e-11/100				
U(IV) oxidation by Fe(III)	(8)	(11)	2.e-11/100				
Sulfur precipitation/dissol.[b]	(10)	(11)	1.4e-11/100				

[a] Rate is assumed to be essentially unlimited by the electron-acceptor (donor-limited experiments)

[b] Rate incorporates (and assumes) a constant surface area

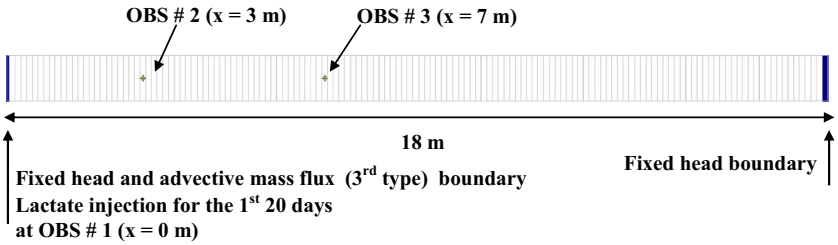

Fig. 2 Model grid and boundary conditions for the 1D model

points. In PHREEQC, a uniform grid resolution of 0.0072 m was used. The flow was assumed to be at steady state; a uniform hydraulic conductivity of 0.432 m/day and a uniform porosity of 0.25 were assumed. Constant head boundaries (first type) were defined for both the influent and effluent end of the column. With the assumed head difference of 0.75 m, this results in a pore water velocity of 0.072 m/day. The total simulation period was defined to be 110 days and a nominal time step size was set to 0.01 days. However, automatic time step size control was invoked by some of the simulators. In PHREEQC, a time step of 0.1 days was used to match the pore water velocity. Unless otherwise noted, a longitudinal dispersivity of 1 m was assumed for the 1D simulations.

2.3.2 2D model

The model domain for the 2D simulation was defined to be 18 m in length and 10.5 m in width with a uniform grid discretization of 0.125 m in both horizontal and vertical directions. Again, slight adjustments to the grid resolution were required for the different simulators to match the exact locations of the observation points (Fig. 3). An injection well was defined at a location 7.25 m downstream of the influent boundary. It was assumed that the injection of a lactate-containing solution occurred at this location at a rate of 0.2 m^3/day during the initial 8 days of the simulation period (see Fig. 3). The lactate-containing solution was injected temporarily into an initially uniform steady state flow field, leading to transient flow conditions. The 2D simulations assumed a longitudinal dispersivity of 1 m and a transverse dispersivity of 0.1 m. The total simulation period was defined to be 60 days with a nominal time step size of 0.01 days. Again, automatic time step size control was invoked by some of the simulators.

2.4 Initial and inflow water composition

The initial conditions that were used to define this benchmark were mostly based on the initial solution composition of the batch experiments conducted by Sani et al. [7], which included 20 mM SO_4^{-2}, 30 mM lactate, 0.4 mM Ca, and 3 mg/L biomass of sulfate reducing bacteria (SRB). Thirty millimolar of PIPES buffer was used in the solution to buffer the pH at 7.2. However, an initial concentration of 6 μM for U(VI) was used (rather than 90 μM), which is more representative of field conditions. The initial carbonate concentrations were set to reflect equilibrium with atmospheric CO_2. Hematite (7.25 mM) was included in the model as Fe(III) hydroxide

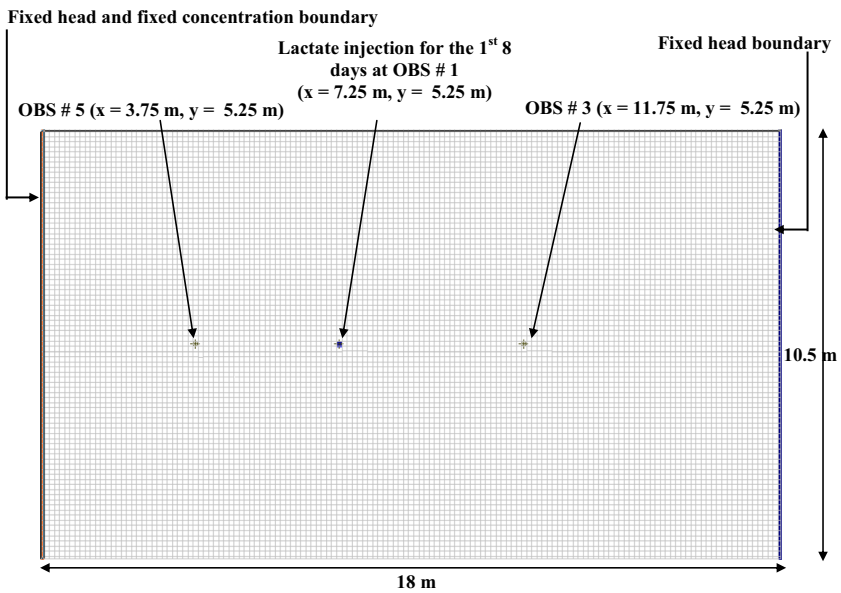

Fig. 3 Model grid and boundary conditions for the 2D model

mineral, directly corresponding to the experimental conditions. The full initial aqueous and mineral concentrations are given in Tables 3 and 4, respectively.

2.4.1 1D model

For the 1D reactive transport model, an advective mass flux (third type) boundary condition was considered for the upstream end of the domain. The water composition that was applied there was defined to contain the same U(VI) concentration as the initial water composition (initial condition). During the first 20 days of the simulation period, the inflow solution also contained lactate (Table 5).

2.4.2 2D model

For the 2D reactive transport model, the upstream boundary was defined as a specified concentration boundary. The lactate-containing solution was added through an injection well rather than at the upstream boundary, as was done in the 1D model. The water composition applied at the upstream boundary was the same as the initial water composition. The water composition applied at the injection well is given in Table 6.

Table 3 Initial aqueous concentrations for the batch simulations, 1D and 2D problems

Chemical component	Concentration (mol/L_{water})
Lactate	3e-7[a]
Acetate	1e-23
Sulfate	0.02
S(−2)	1e-8
Fe(2)	1e-23
Fe(3)	1.e-11 (Equilibrium with hematite)
U(6)	1e-6
Ca	0.00042
Mg	0.004
C(4)	1.7e-7
U(4)	1e-23
Na	0.06 (Charge balanced)
Cl	8.2e-04
Pip	0.03[b]
pH	7.2

[a] 3e-10 M of lactate is specified at the first grid cell, and 3e-7 M was specified at the rest of the grid domain

[b] "Pip" stands for the PIPES [piperazine-N,N-bis(2-ethanesulfonic acid)] which was added at a concentration of 0.03 M to maintain the buffer capacity of the medium. The speciation reaction is as follows: Pip-+H+ =HPip log_k 7.2

Table 4 Initial mineral concentrations for the batch simulations, 1D and 2D problems

Mineral	Concentration (mol/L_{water})
Hematite	7.25E-03
Uraninite	0
Sulfur	0
Mackinawite	0
Siderite	0

2.5 Numerical model implementation

In this benchmark problem set, four different simulators (PHREEQC, PHT3D, MIN3P, and TOUGHREACT) were used to compare the simulation results and determine whether biogeochemical reaction networks and the coupling between transport and reaction kinetics are captured in the same manner by the different codes. First, the ability of the codes to capture the complex biogeochemical reaction system is tested by the numerical simulation of batch experiments. The code inter-comparison for transport and coupling between reaction kinetics and transport were then tested by 1D and 2D

Table 5 Specified aqueous concentration of the inflowing water at the left end of the domain for the 1D model

Chemical component	Specified Concentration of inflowing water (mol/L_{water})
Lactate	0.03[a]
Acetate	1e-23
Sulfate	0.02
S(−2)	1e-23
Fe(2)	1e-23
Fe(3)	1.3e-12 (Equilibrium with hematite)
U(6)	1e-6
Ca	0.00042
Mg	0.004
C(4)	0.0001193[b]
U(4)	1e-23
Na	0.07914 (Charge balanced)[c]
Cl	8.20E-04
Pip	0.03
pH	7.2

[a] 0.03 M of lactate is injected for the first 20 days of simulation; then the lactate concentration is specified as 3e-10 M for the rest of the simulation period

[b] 0.0001193 M of C(4) is specified for the first 20 days of simulation, then to satisfy the charge balance, the concentration is specified as 0.000140 M for the rest of the simulation period

[c] Charge balance is maintained on Na, where the charge balanced concentration is 0.07914 M for the first 20 days of simulation and then 0.04891 M for the rest of the simulation period

Table 6 Aqueous concentration of the inflowing water at injection well for the 2D model

Chemical component	Specified concentration of inflowing water (mol/L_{water})
Lactate	0.03[a]
Acetate	1e-23
Sulfate	0.02
S(−2)	1e-23
Feii	1e-23
Fe(3)	1.3e-12 (Equilibrium with hematite)
U(6)	1e-23
Ca	0.00042
Mg	0.004
C(4)	1.187e-04[b]
U(4)	1e-23
Na	0.07914 (Charge balanced)[c]
Cl	8.20E-04
Pip	0.03
pH	7.2

[a] 0.03 M of lactate is injected for the first 8 days of simulation; then the lactate concentration is specified as 3e-10 M for the rest of the simulation period

[b] 1.187e-04 M of C(4) is specified for the first 8 days of simulation, then to satisfy the charge balance, the concentration is specified as 1.134e-04 M for the rest of the simulation period

[c] Charge balance is maintained on Na, where the charge balanced concentration is 0.07914 M for the first 8 days of simulation and then 0.04891 M for the rest of the simulation period

simulations. As the spatial weighing schemes for the advection term and numerical dispersion effects can play an important role on the results, various numerical solution options were investigated along with the comparison of different codes. Those investigated options included spatial and temporal discretization levels and schemes as well as the numerical solution schemes. Comparison of the numerical solution schemes for advective transport implemented in the different simulators are listed as:

- Third-order total-variation diminishing (TVD) scheme based on the ULTIMATE algorithm (PHT3D), as discussed in Zheng and Wang [19]
- Upstream weighting finite difference method (PHT3D, MIN3P, and TOUGHREACT), as discussed in Zheng and Wang [19]
- Implicit time weighting with a van-leer flux limiter (MIN3P), as discussed in van Leer [20]
- Upwind for advective transport implemented as the mixing cell technique (PHREEQC), basically corresponding to an explicit finite difference method with CFL=1, which is free of numerical dispersion, as discussed in Parkhurst and Appelo [9]

MODFLOW 2005 [21] was used as the flow model to calculate the velocity fields for reactive transport simulations with PHT3D. MIN3P has its own flow model which was used in the reactive transport simulations for the 1D and 2D cases. Since dispersion is not explicitly considered in the TOUGHREACT code, as described by Xu et al. [12, 13], cases with dispersion are compared only between PHREEQC (for the 1D problem), PHT3D, and MIN3P codes.

3 Results and discussion

3.1 Numerical simulation of batch experiments

The first part of the model intercomparison was performed to compare the ability of the codes to simulate the complex reaction network in the absence of any flow and solute transport. The results of these batch-type simulations are shown in Fig. 4 for the most relevant aqueous species, together with the data that were measured in the original batch experiments of Sani et al. [7] and the TOUGHREACT simulation results obtained by Spycher et al. [8]. The simulation and experimental results illustrate the temporal concentration variations that are induced by the reduction of sulfate during the microbial transformation of lactate to acetate in conjunction with U(VI) reduction and the formation of UO_2 precipitates. Once lactate was depleted, precipitated UO_2(bio) was reoxidized by hematite while redox conditions remained reducing and sulfide was still present (reaction 8). As discussed in Spycher et al. [8] the oxidation of sulfide by hematite (reactions 9 and 10) was directly competing with UO_2 reoxidation (reaction 8). Therefore an accurate quantification of the relative rates of these reactions play a key role for the potential of precipitated uraninite to be reoxidised [8], and for its mobility towards environmental receptors.

The comparison of the results with the measured data demonstrates that the simulations employing the proposed reaction network capture the important thermodynamic and kinetic constraints that influence the biogenic UO_2 reoxidation by Fe(III) hydroxides under sulfate reducing conditions (Fig. 4). Figure 4 shows that the results of the numerical solutions for U(VI), sulfate, acetate, lactate, HS^-, and Fe(II) species using the different simulators coincide very closely. Slight deviations occur for TOUGHREACT compared to the other codes, mostly for U (VI) species, after about 35 days. The simulation results, in particular for the timing of the reversal in the U (VI) trend, showed to be extremely sensitive to the combined effect of the reactions.

3.2 Numerical simulation of 1D model

For the second part of the benchmark study (1D reactive transport), the performance of the different simulators was first

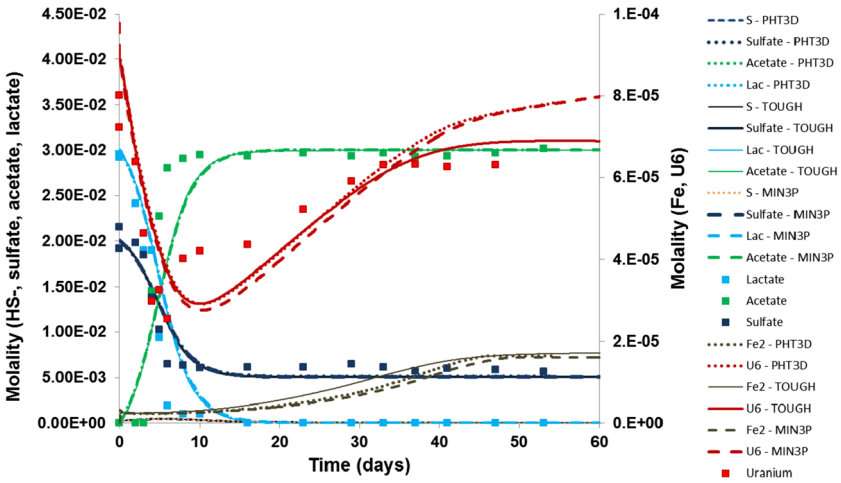

Fig. 4 Comparison of simulated concentrations for U(VI), sulfate, acetate, lactate, HS^-, and Fe using PHT3D, TOUGHREACT and MIN3P simulators. Symbols are the batch experimental data points from Sani et al. [7]

assessed for the case of non-reactive transport. Selected results are illustrated in Fig. 5, which shows a comparison of simulated lactate concentrations in the absence of any degradation reactions. The simulated concentrations are shown for three observation points located at 0 m (OBS1), 3 m (OBS2) and 7 m (OBS3) downgradient of the model boundary (as shown in Fig. 2). Based on the comparison of the simulation results with different simulators, it is seen that PHT3D, PHREEQC and MIN3P results agree very well, capturing the advection-dispersion process in the benchmark problem.

For the reactive transport simulations, the results of the three different codes are shown in Fig. 6 for selected aqueous species (lactate, acetate, Fe(II), U(VI), HS^-, and HCO_3^-). The results illustrate for selected observation points the reduction of sulfate by microbial degradation of lactate to acetate and the reduction of hematite and U(VI) by sulfide with sulfur as one of the end products. The observed peaks for acetate, HS^-, Fe(II), HCO_3^- species correspond to the occurrence of these microbial reactions, which can proceed where sufficient lactate is available as it migrates into the column from the upstream boundary. After lactate is no longer injected, concentrations gradually decrease due to degradation and dilution. The reaction-induced decrease in lactate concentration due to microbial degradation to acetate can be seen when the corresponding peaks in Fig. 6 are compared with the peaks in Fig. 5 of the non-reactive tracer results. The decrease in U(VI) concentration is primarily due to the bioreduction by sulfide, and the increase is partly due to the reoxidation of biogenic UO_2 by hematite as well as the injection from the incoming water at the upstream boundary combined with the effect of

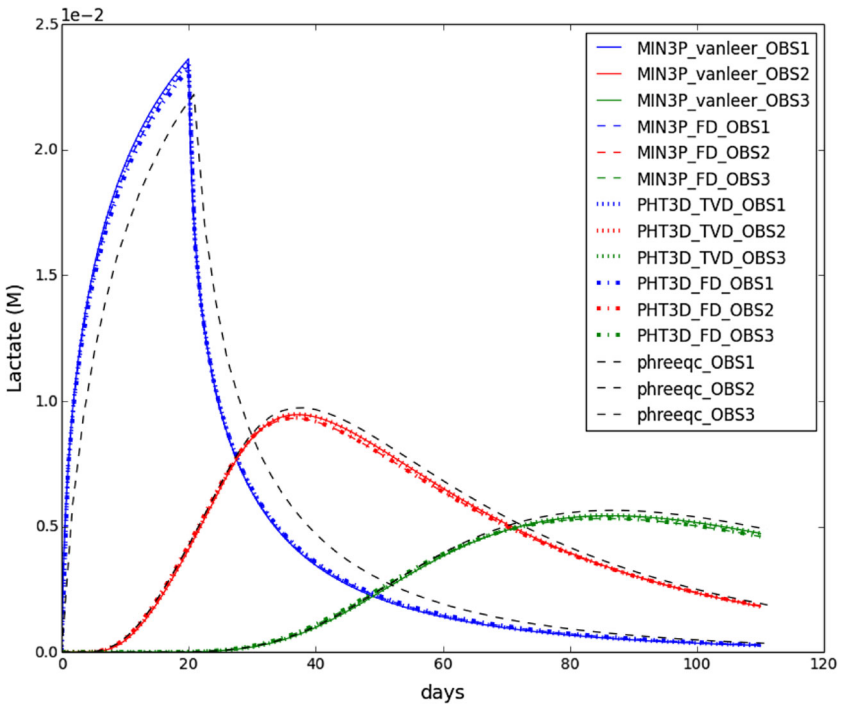

Fig. 5 Comparison of tracer concentrations at observation points 1, 2, and 3 for all simulators using different solution schemes for the 1D transport problem considering dispersion using 1 m longitudinal dispersivity

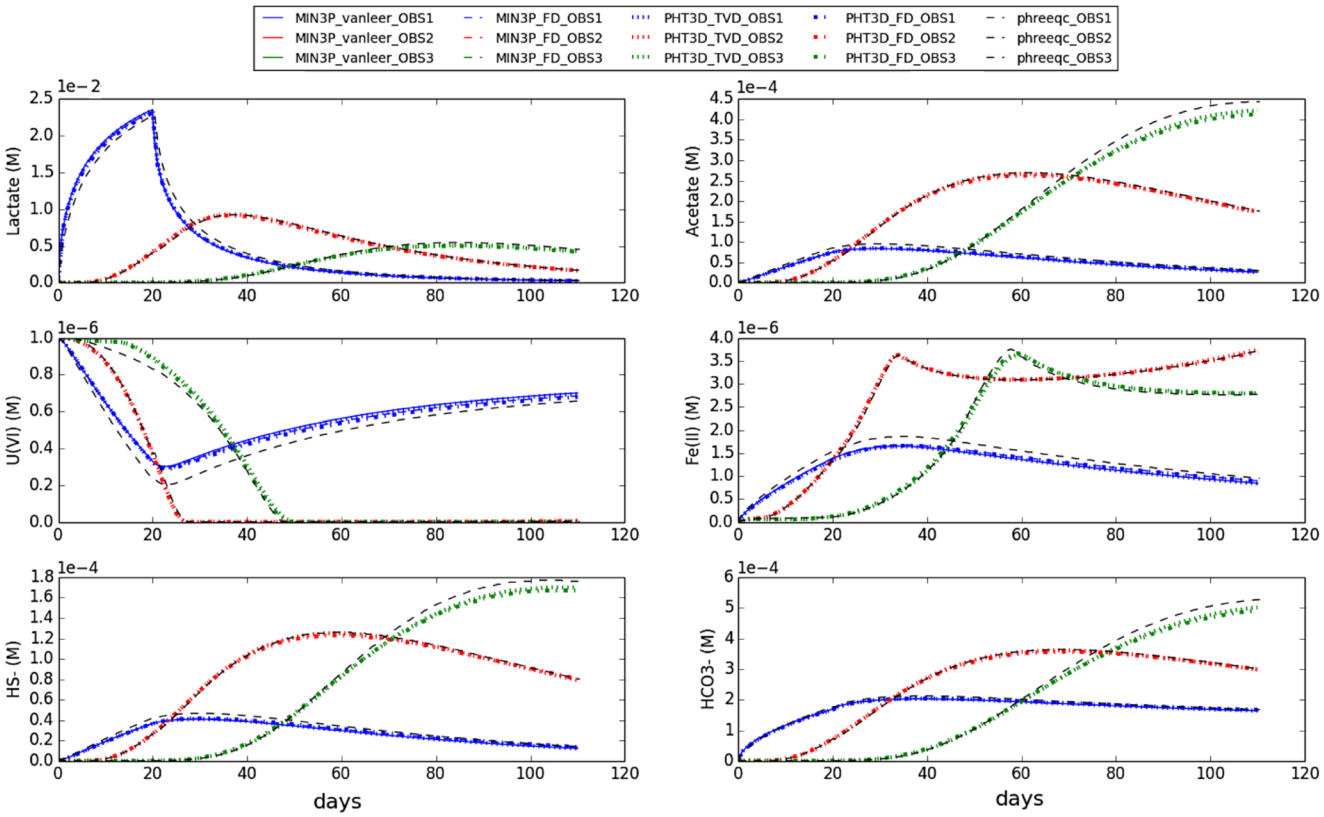

Fig. 6 Comparison of key aqueous species (lactate, acetate, U(VI), HS^-, Fe(II), and HCO_3^-) concentrations at observation points 1, 2, and 3 using PHREEQC, PHT3D, and MIN3P reactive transport codes using different solution schemes for the 1D reactive transport problem considering 1-m dispersivity

mixing by dispersion. Figure 6 shows that the results of the different simulators PHT3D, PHREEQC and MIN3P agree very well when a longitudinal dispersivity of 1 m is considered, indicating that transport, the biogeochemical reaction system, and accurate coupling between the two has been verified for the codes participating in this benchmark.

After consistency of results among the participating codes was achieved, the assessment was extended to investigate the impact of different solution schemes for the various simulators (PHT3D: TVD and upstream weighting scheme; MIN3P: Van Leer flux limiter and upstream weighting scheme; PHREEQC: explicit finite difference scheme that is forward in time, central in space for dispersion, and explicit upwind with CFL=1 for advective transport). This comparison showed that numerical dispersion effects can in some instances play an important role in deteriorating the accuracy of results. While in the case of a longitudinal dispersivity of 1 m all codes showed a consistent agreement of simulated concentrations independent of the employed solution scheme (Fig. 6), this was not the case when hydrodynamic dispersion was omitted. The comparison for this case, which also included results from TOUGHREACT simulations, showed an excellent agreement among all codes when upstream weighting was employed. This was the case for both non-reactive transport (Fig. 7a) and reactive transport (Fig. 8). In contrast, when different solution schemes were used (other than upstream) for the dispersion-free case, results showed substantial discrepancies among the codes (Fig. 9). Figures 7b and 9 suggest that PHREEQC provides a dispersion-free solution, which was most closely matched by the PHT3D solution that applied the TVD scheme with explicit time weighting, and the MIN3P solution that employed the van Leer scheme with implicit time weighting. Although the results obtained by all codes compared very well among each other when employing upstream weighting, these results showed strong deviations from the dispersion-free PHREEQC solutions. Results obtained using upstream weighting also substantially differed from PHT3D and MIN3P solutions that were obtained with advection schemes designed to minimize numerical dispersion. Upstream weighting is well-known to perform poorly for advection-dominated conditions under transient conditions and thus also for advection-only cases (e.g., [22]). The fact that significant numerical dispersion introduced by upstream weighting (and depending on grid-resolution, also by other schemes) results in artificial mixing and over-prediction of reaction rates, has been discussed previously (e.g., [23]). While in the no-dispersion case, the principal reaction patterns were captured by all solutions, the comparison illustrates the

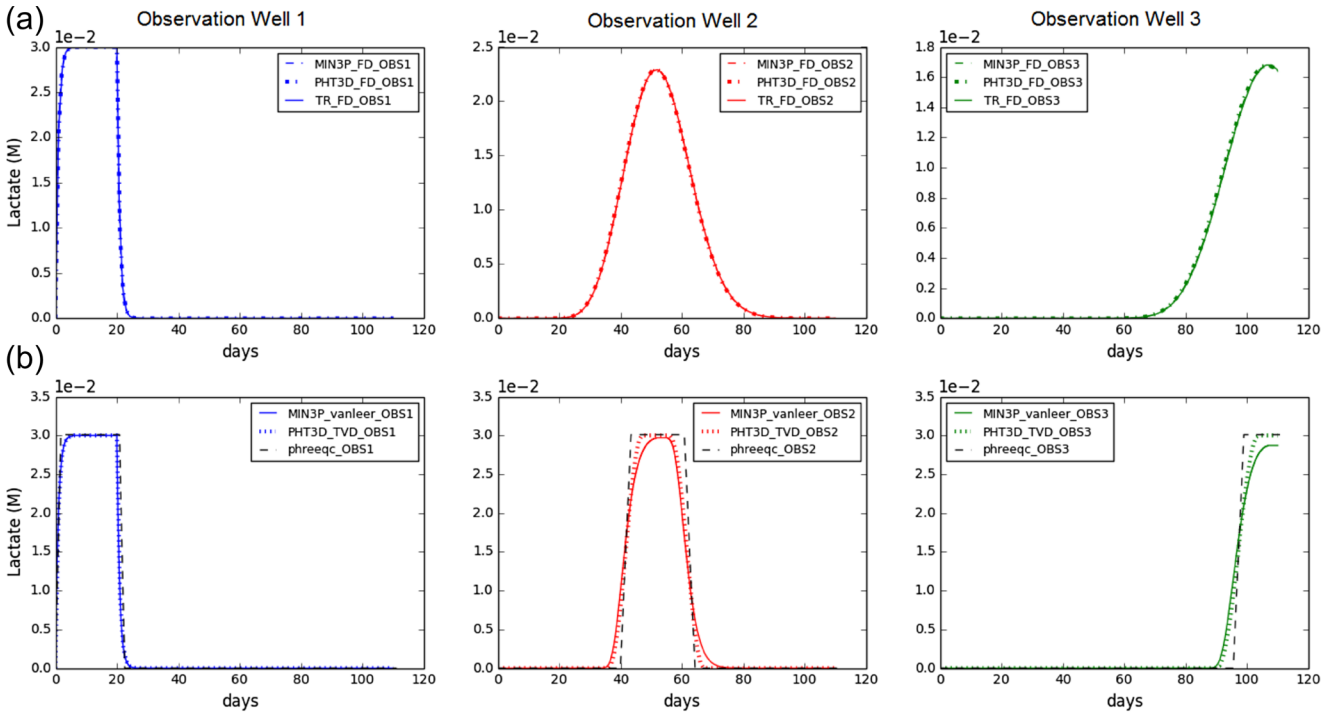

Fig. 7 Comparison of tracer concentrations at observation points 1, 2, and 3 for (**a**) PHT3D, MIN3P, and TOUGHREACT codes using upstream weighting schemes, and (**b**) PHT3D, MIN3P, and PHREEQC codes using alternative solution schemes for the 1D transport problem considering no dispersion cases

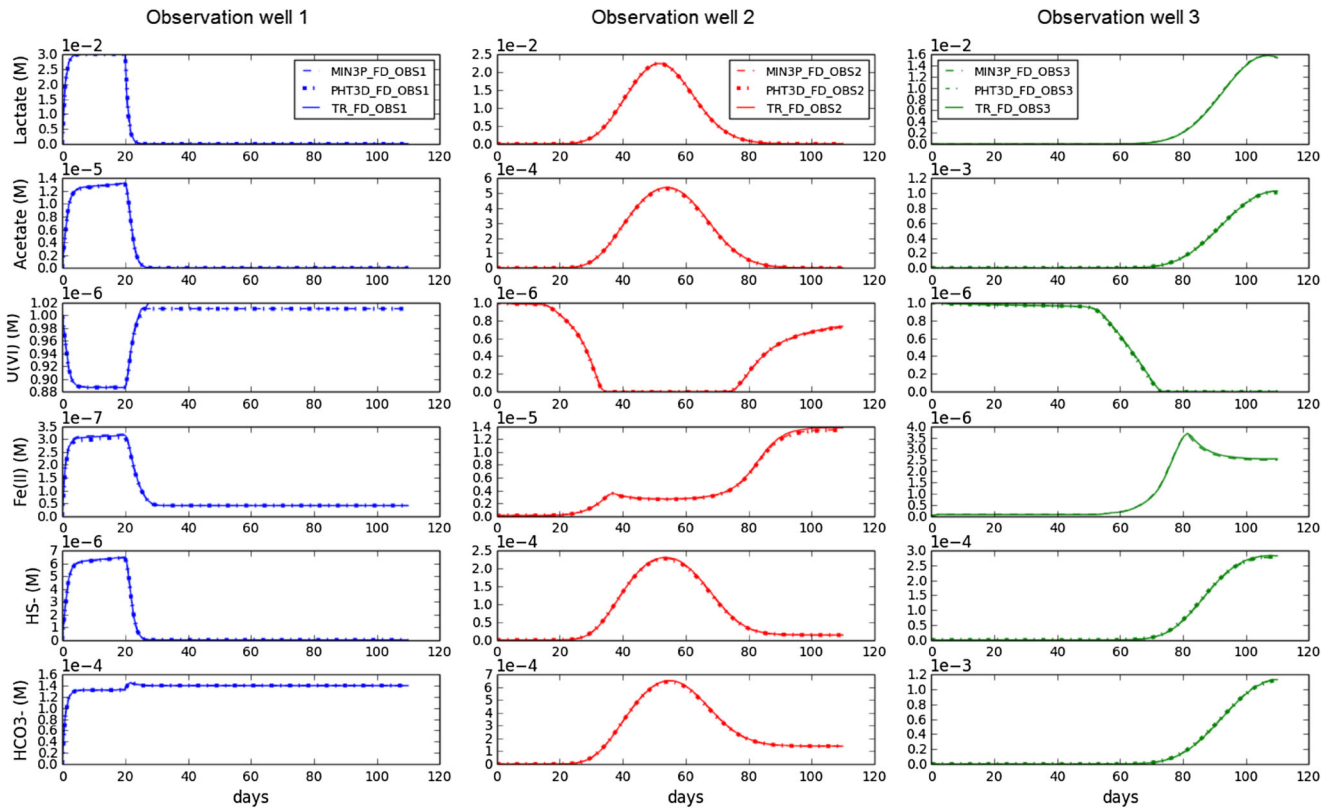

Fig. 8 Comparison of key aqueous species (lactate, acetate, U(VI), HS^-, Fe(II), and HCO_3^-) concentrations at observation points 1, 2, and 3 using PHT3D, MIN3P, and TOUGHREACT codes using upstream weighting schemes for the 1D transport problem considering no dispersion

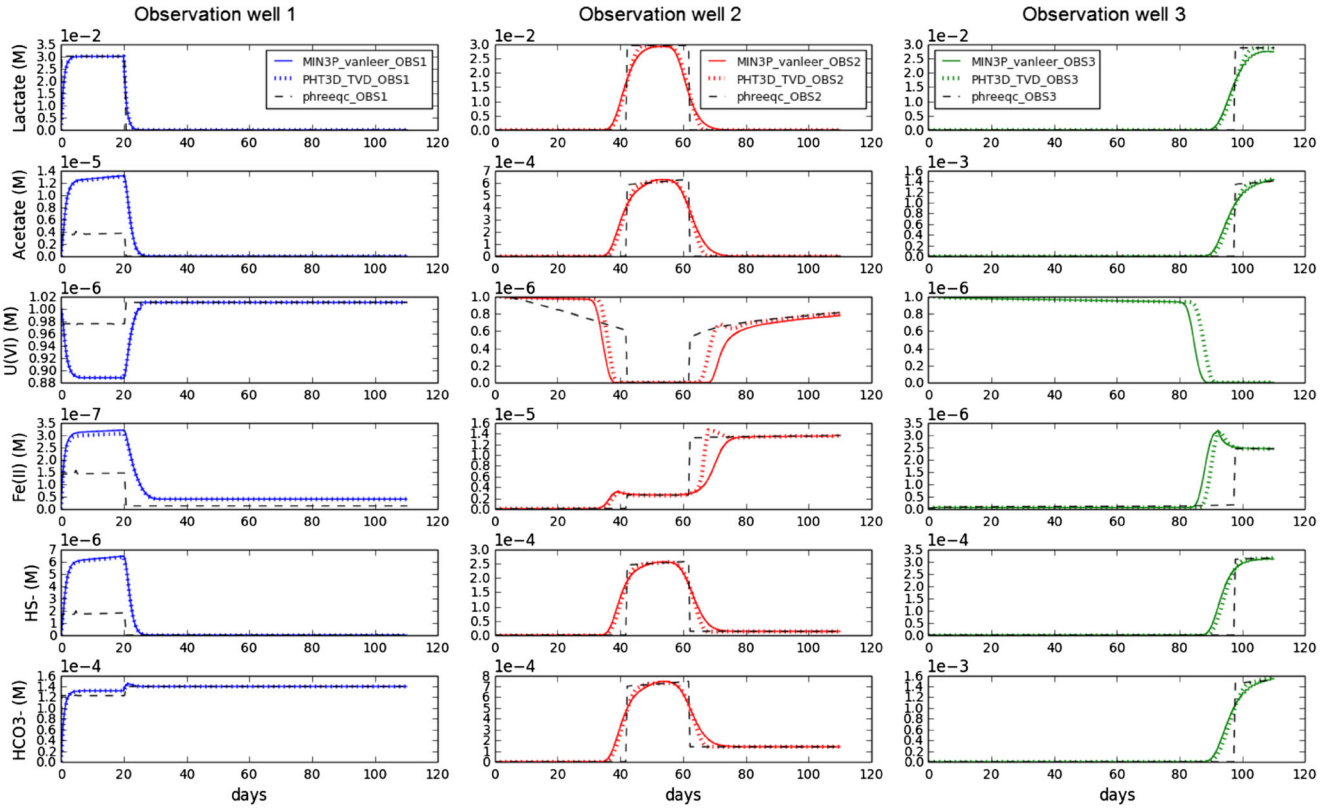

Fig. 9 Comparison of key aqueous species (lactate, acetate, U(VI), HS^-, Fe(II), and HCO_3^-) concentrations at observation points 1, 2, and 3 using PHREEQC, PHT3D, and MIN3P reactive transport codes using different solution schemes (other than upstream) for the 1D transport problem considering no dispersion

significant impact that numerical solution schemes may have on the results (Figs. 8 and 9). However, it should be noted that, in principle, the dispersion-free case is not realistic for most subsurface simulation problems, neither on the field-scale nor on the laboratory-scale. It should also be noted that the temporal and spatial discretization used in the PHREEQC simulations were not the same as in the other codes, which explains the differences that can be observed at the inflow end (Fig. 9). For the PHREEQC simulations, it was necessary to use a finer grid, which led to reduced residence time in the inflow cell. When using a coarser grid aligned with the discretization of the other codes, PHREEQC requires larger time steps to maintain the specified flow velocity. Using this approach, it was not possible to achieve a stable and oscillation free solution.

In this benchmark, the grid discretization was successively reduced until all codes (independent of the solution scheme) agreed closely for the case where a dispersivity of 1 m was considered. Grid convergence was effectively obtained for a grid size of 0.125 m. When coarser grid resolutions were used for the problem, upstream weighting schemes showed deviations from the other schemes even for the simulations with a dispersivity of 1 m (data not shown). Although the influence of numerical dispersion can in principle be minimized with a finer grid resolution and corresponding time step adjustments when lower dispersivity cases are studied, this may result in an excessive computational demand for the FD schemes that are better overcome with higher-order advection schemes.

3.3 Numerical simulation of 2D model

The third part of the benchmark problem replicates the coupled transport and reaction patterns that would occur in a field-scale remediation scenario. Lactate that is injected for a period of 8 days at the start of the simulation period is spreading radially from the injection well, as illustrated in Fig. 10. Concentration contours for several aqueous species (lactate, acetate, U(VI), Fe(II), HS^-, and uraninite) are shown after 10, 20, and 40 days after the start of the simulation, i.e., 2, 12, and 32 days after the end of the lactate injection, respectively. These results are compared for the simulators PHT3D (solid lines) and MIN3P (dashed lines) (Fig. 10). The figure also illustrates the spatial extent of the uranium immobilization that was induced by the lactate injection. It should be noted that enhanced mixing of the injected lactate solution with uranium-containing groundwater, progressing from the upstream boundary, leads to preferential uraninite precipitation upgradient of the injection well, resulting in the observed "moon shape" (Fig. 10). Compared to batch and 1D simulations, the 2D case with its radial flow field near the injection well provided additional challenges in terms of accurately

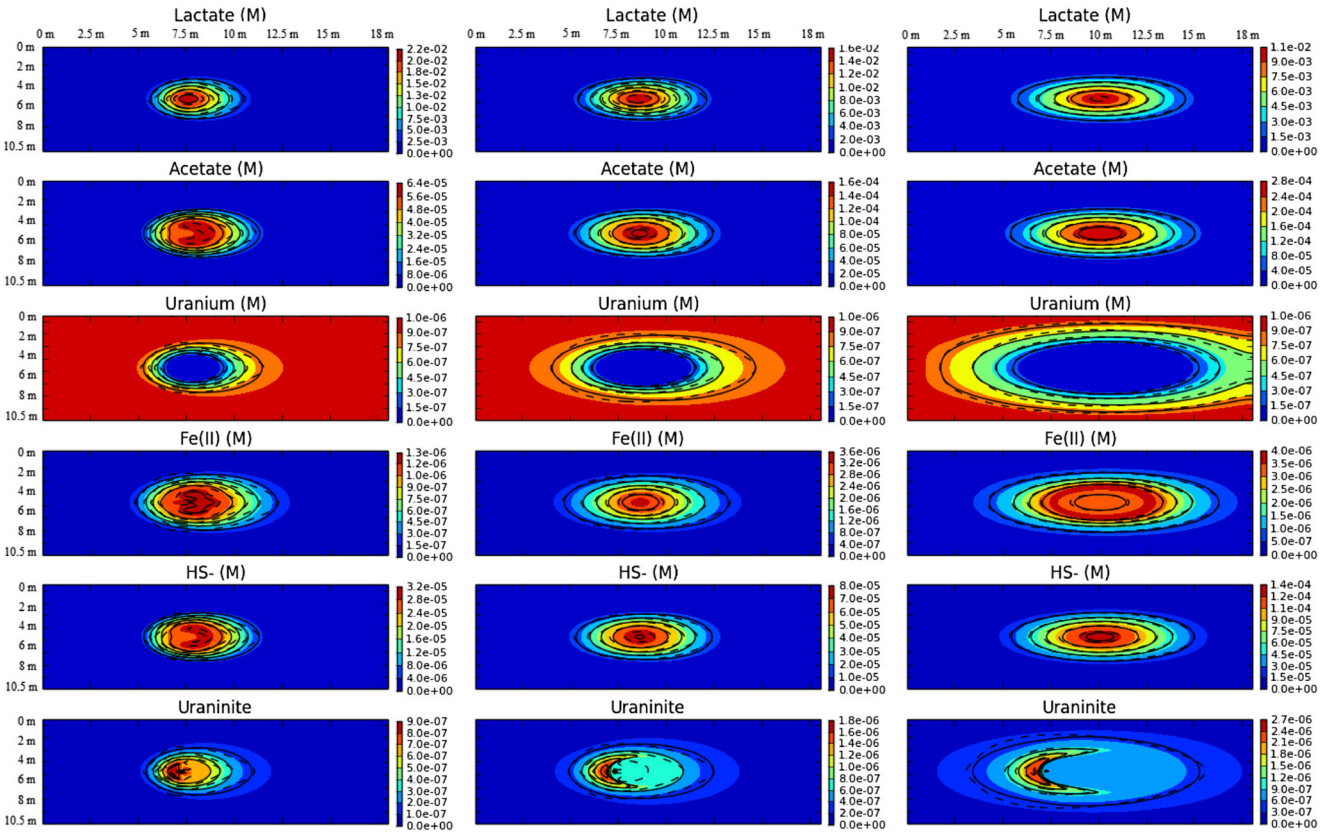

Fig. 10 Concentration contours of lactate, acetate, U(VI), Fe(II), HS^-, and uraninite after 10, 20, and 40 days after the start of the simulation, i.e., 2, 12, and 32 days after the end of the lactate injection, respectively. *Solid lines* and the *color scale* indicate results obtained from PHT3D simulator. *Dashed lines* correspond to MIN3P simulator results

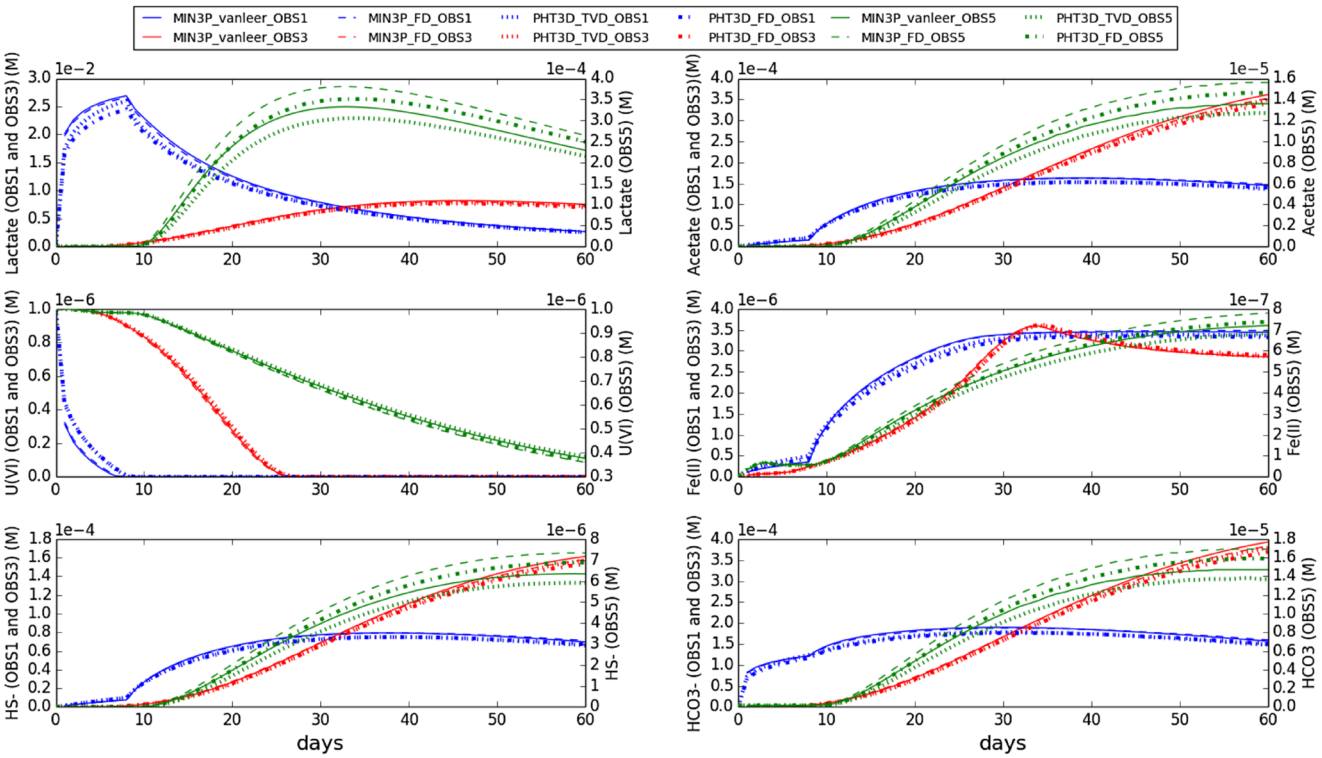

Fig. 11 Comparison of key aqueous species (lactate, acetate, U(VI), HS^-, Fe(II), and HCO_3^-) concentrations at observation points 1, 3, and 5 using PHT3D and MIN3P reactive transport codes using different solution schemes for the 2D reactive transport problem

computing coupled transport and reactions on a Cartesian grid. Figure 11 shows the comparison of the simulated concentrations for the different codes at the three observation points (as shown in Fig. 3). It is seen from the results that both simulators, PHT3D and MIN3P produce nearly identical results for the key aqueous species, showing that the complex reaction network including multiple and competing kinetic reactions coupled with the 2D transport is well captured by both simulators, when a longitudinal dispersivity of 1 m and a transverse dispersivity of 0.1 m are employed in combination with a 0.125-m grid resolution. Nevertheless, there are some noticeable differences between the codes at observation point 3, especially for lactate, acetate, Fe(II), HS^-, and HCO_3^-. At that location, which is furthest away from the injection well, simulated concentrations are significantly lower compared to OBS1 and OBS2 (see Fig. 11). The lower concentrations that prevail at the dispersive front, where mixing of different waters occurs, cause concentration trends and differences to be more pronounced. Such differences were not evident in the 1D case. To further explore this issue, the comparison of the simulation results was again extended to compare different solution schemes for both simulators (Fig. 11). It can be inferred that due to the explicit time weighting implementation, the least dispersive solution is achieved by PHT3D using the TVD scheme. However, an acceptable solution can also be achieved with the GIM, as long as a flux limiter scheme is implemented (MIN3P results).

Note that with the grid discretization being refined to 0.125 m, the computational times for the 2D simulations increased significantly and high performance parallel computing capabilities were used. Therefore, further grid refinement to reduce numerical dispersion effects was not deemed reasonable with the considered complex reaction chemistry, strong interdependency of the reaction processes, and the sensitivity of the solution chemistry to the mixing of the waters at the dispersive front.

4 Summary and conclusions

In this study, a benchmark problem set was developed for a mixing controlled reactive transport problem. It was used to illustrate how different model formulations compare, and whether the various codes can cope with the complex biogeochemical reaction kinetics. The first part of the proposed benchmark problem consists of the simulation of the original batch experiments using the same biogeochemical reaction network as developed by Spycher et al. [8]. The second and third parts extend the batch simulations to 1D and 2D reactive transport problems, respectively, employing the same ambient and inflow hydrochemical composition as the initial aqueous composition used in the first part.

Four different reactive transport simulators: PHREEQC, PHT3D, MIN3P, and TOUGHREACT were used in this study and simulation results were compared. The results show that all codes were able to capture the complex biogeochemical reaction network which included parallel, sequential, and competing reaction kinetics. The coupling between transport and the kinetic reaction system was also successful for all codes. As the study showed that this benchmark was strongly affected by mixing of different waters at the dispersive front, the comparison of the results were then extended to include different solution schemes available in the different simulators. The results showed that for the defined grid-resolution level, the solution subject to the lowest degree of numerical dispersion was obtained with SNIA using a TVD scheme, while the GIM using an implicit van Leer flux limiter also provided an acceptable solution. When upstream weighting was used, the results showed a very good agreement among all codes, capturing coupled reactive transport processes in the same manner. However, for the dispersion free test condition, this approach introduced significant numerical dispersion resulting in deviations in all codes when compared to other schemes (PHT3D with TVD; MIN3P with flux limiter). These discrepancies were amplified in the 2D case, especially in regions with low concentrations further away from the injection point, even when longitudinal and transverse dispersivities were considered. Such differences in the simulation results could be minimized with further grid refinement; however, this may not be practical due to computational constraints associated with the complex reaction network.

Acknowledgments We are thankful to David Parkhurst for his help on clarification of rate expressions in PHREEQC. We thank Nicolas Spycher for his help on TOUGHREACT database and input files that assisted in running reactive transport simulations for TOUGHREACT code, which was also useful in setting-up MIN3P database files.

Conflict of interest The authors declare that they have no conflict of interest.

References

1. Lloyd, J.R., Lovley, D.R.: Microbial detoxification of metals and radionuclides. Curr. Opin. Biotechnol **12**, 248–253 (2001)
2. Gavrilescu, M., Lucian, V.P., Cretescu, I.: Characterization and remediation of soils contaminated with uranium. J. Hazard. Mater **163**, 475–510 (2009)
3. Craft, E.S., Abu-Qare, A.W., Flaherty, M.M., Garofolo, M.C., Rincavage, H.L., Abou-Donia, M.B.: Depleted and natural uranium: chemistry and toxicological effects. J Toxicol Env Heal B **7**, 297–317 (2004)
4. Lovley, D.R., Phillips, E.J., Gorby, Y.A., Landa, E.R.: Microbial reduction of uranium. Nature **350**, 413–416 (1991)
5. Lovley, D.R., Phillips, E.J.: Bioremediation of uranium contamination with enzymatic uranium reduction. Environ. Sci. Technol **26**, 2228–2234 (1992)

6. Anderson, R.T., Vrionis, H.A., Ortiz-Bernad, I., Resch, C.T., Long, P.E., Dayvault, R., Lovley, D.R.: Stimulating the in situ activity of Geobacter species to remove uranium from the groundwater of a uranium-contaminated aquifer. Appl. Environ. Microbiol **69**, 5884–5891 (2003)
7. Sani, R.K., Peyton, B.M., Amonette, J.E., Geesey, G.G.: Reduction of uranium(VI) under sulfate-reducing conditions in the presence of Fe(III)- (hydr)oxides. Geochim. Cosmochim. Acta **68**, 2639–2648 (2004)
8. Spycher, N., Issarangkun, M., Stewart, B., Sengor, S.S., Belding, E., Ginn, T.R., Peyton, B., Sani, R.K.: Biogenic Uraninite Precipitation and its Reoxidation by Iron(III)(Hydr)oxides: A Reaction Modeling Approach. Geochim. Cosmochim. Acta **75**, 4426–4440 (2011)
9. Parkhurst, D.L., Appelo, C.A.J.: User's guide to PHREEQC (version 2) – a computer program for speciation, batch-reaction, one-dimensional transport, and inverse geochemical calculations, Denver, CO (1999)
10. Prommer, H., Barry, D.A., Zheng, C.: MODFLOW/MT3DMS-based reactive multicomponent transport modeling.pdf. Ground Water **41**, 247–257 (2003)
11. Mayer, K.U., Frind, E.O., Blowes, D.W.: Multicomponent reactive transport modeling in variably saturated porous media using a generalized formulation for kinetically controlled reactions. Water Resour. Res **38**, 13–1 (2002)
12. Xu, T., Spycher, N., Sonnenthal, E.L., Zhang, G., Zheng, L., Pruess, K.: TOUGHREACT Version 2.0: a simulator for subsurface reactive transport under non-isothermal multiphase flow conditions. Comput. Geosci **37**, 763–774 (2011)
13. Xu, T., Spycher, N., Sonnenthal, E., Zheng, L., Pruess, K.: TOUGHREACT user's guide : A simulation program for non-isothermal multiphase reactive transport in variably saturated geologic media, Version 2.0., Berkeley, CA (2012)
14. Fang, Y., Yabusaki, S.B., Morrison, S.J., Amonette, J.P., Long, P.E.: Multicomponent reactive transport modeling of uranium bioremediation field experiments. Geochim. Cosmochim. Acta **73**(20), 6029–6051 (2009)
15. Park, J., Sanford, R.A., Bethke, C.M.: Microbial activity and chemical weathering in the Middendorf aquifer. South Carolina. Chem. Geol **258**, 232–241 (2009)
16. Yeh, G.T., Tripathi, V.S.: A critical evaluation of recent developments in hydrogeochemical transport models of reactive multichemical components. Water Resour. Res **25**, 93–108 (1989)
17. Engesgaard, P., Kipp, K.L.: A geochemical transport model for redoxcontrolled movement of mineral fronts in groundwater flow systems: A case of nitrate removal by oxidation of pyrite. Water Resour. Res **28**, 2829–2843 (1992)
18. Steefel, C.I., Arora, B., Appelo, C.A.J., Hammond, G., Jacques, D., Kolditz, O., Lagneau, V., Lichtner, P.C., Mayer, K.U., Meussen, H., Molins, S., Parkhurst, D.L., Shao, H., Simůnek, J., Lee, J., Van der Yabusaki, S.B., Yeh, G.T.: Reactive transport codes for subsurface environmental simulation. Comput. Geosci (2014). doi:10.1007/s10596-014-9443-×
19. Zheng, C., Wang, P.P.: MT3DMS: A Modular Three-Dimensional Multispecies Transport Model for Simulation of Advection, Dispersion and Chemical Reactions of Contaminants in Groundwater Systems; Documentation and User's Guide, Contract Report SERDP-99-1. U.S. Army Engineer Research and Development Center, Vicksburg, MS (1999)
20. van Leer, B.: Towards the ultimate conservative scheme. II Monotonicity and conservation combined in a second order scheme. J. Comp. Phys **14**, 361–370 (1974)
21. Harbaugh, A.W.: MODFLOW-2005, the US Geological Survey modular ground-water model: The ground-water flow process, p. 6-A16. US Department of the Interior, US Geological Survey, Reston, VA, USA (2005)
22. Zheng, C., Bennett, G.D.: Applied Contaminant Transport Modeling. John Wiley & Sons, New York (2002)
23. Cirpka, O.A., Frind, E.O., Helmig, R.: Numerical simulation of biodegradation controlled by transverse mixing. J. Contam. Hydrol **40**, 159–182 (1999)